The Role of Acoustic-Reynolds Stress in the Flame-Acoustic Coupling of Combustion Instability in a Dump Combustor

C. Balaji[1], S.R. Chakravarthy[2], K. Ashwin[·, 2]

[1]Metacomp Technologies Pvt. Ltd., Chennai-600020, India
[2]National Center for Combustion Research and Development & Department of Aerospace Engineering, Indian Institute of Technology Madras, Chennai-600036, India

Abstract
Combustion instability in a laboratory scale dump combustor is examined by implementing incompressible large eddy simulations of an acoustically coupled turbulent reacting flow for various Reynolds numbers with fuel injection at the step. The full compressible Navier-Stokes equations are decomposed using multi-scale analysis to yield an incompressible base flow to leading order and linearized Euler equations for acoustics to first order. The coupling terms are identified to be flow dilatation for acoustic energy and acoustic Reynolds stress (ARS) for flow momentum. The numerical simulations capture flow-acoustic lock on, which signifies the onset of combustion instability, marked by a shift in the dominant frequency. The coupled simulations also show a compact flame and distinctly different flow field upstream of the step than when acoustically decoupled, indicating the role of the ARS.

Introduction
Combustion instability has been a sustaining precarious consequence of the non-linear interaction between the unsteady heat release rate fluctuations, vortex dynamics and acoustics leading to the production, growth and sustenance of high amplitude sound in low NOx combustors. Some of the significant mechanisms of combustion instability involve vortex shedding [1] and equivalence ratio fluctuations [2], both leading to heat release rate fluctuations that act as a source to the acoustic field.
The acoustic-flame-flow interaction involved in combustion instability is governed by the compressible Navier-Stokes equations. Many investigators have solved the compressible Navier-Stokes equations directly to study combustion instability in practical combustors, e.g., [3, 4]. Further, approaches such as URANS [5]/LES [6] are also performed to compute flows that are prone to combustion instability. A hybrid approach involving compressible LES and a Helmholtz acoustic solver is also reported [7, 8].
These computations based on compressible Navier-Stokes equations can provide a reasonably accurate description of the underlying flow physics. However, the computational efforts become more taxing when trying to compute practical turbulent flow fields. This motivates the development of reduced order modeling approaches to compute these flows. In a majority of the reduced order models, the linear evolution equations for the acoustic field are considered, and the unsteady heat release rate from the flame is modeled to act as a source of the acoustic field, in a somewhat ad hoc manner. In these approaches the acoustic variable, usually the acoustic velocity, is related to the heat release rate to close the acoustic equation. The acoustic equations are generally solved in the frequency domain and the unsteadiness of the flame (or its heat release rate) in response to the acoustic velocity at the inlet in the frequency range of interest is computed or measured first and subsequently used in the acoustic evolution equation. This is known as the flame transfer function (FTF). Recently, Boudyet al. [9] adopted the flame-describing function (FDF) obtained at different amplitudes. Vortex based flame models are used when the dominant mechanism for heat release rate fluctuations that drives duct acoustics are due to large scale vortical structures that are formed in the flame stabilizing regions [10-12].

The underlying presumption in most of these models is that of the same characteristic time scales of the flame and acoustics, indicating prevalent instability mode. However in practical combustors, it is observed that the flame dynamically evolves as it interacts with the acoustic field [13-15] and their time scales are observed to approach each other [15] as the system enters into instability mode.

Wu et al. [16] considered the dynamic evolution of the flame as it got coupled with the duct acoustics and showed that the flame drove the acoustics by inducing a jump in the longitudinal velocity and the acoustics in turn affected the flame through the global acceleration term. Tyagi et al. [17] also considered the simultaneous evolution of a non-premixed flame in the Burke-Schumann geometry along with the duct acoustics. The present work adopts a simultaneous multiple time and length scales framework where the flow/flame evolves at a longer time scale and shorter length scale while the acoustics evolves at a shorter time scale and longer length scale. This engenders flow dilatation to act as the source to the acoustic field while the acoustic Reynolds stress (ARS) closes the feedback loop by affecting the momentum of the flow.
Acoustics interacts with the base flow in the interior region through the ARS [18,19]. The mixing or "stirring" characteristics of the ARS is highlighted by Nyborg [18], who also points out the wide application

· Corresponding author: ashwinkannan92@gmail.com

of the ARS in areas of heat transfer, surface reaction, biological cell changes etc., in enhancing the rate at which these processes occur. Tanabe et al. [20] investigated the importance of ARS in enhancing the evaporation rate.

The present paper highlights the significance of ARS in causing intense mixing between reactants and promoting combustion by churning out large-scale vortical structures as the time scales approach each other, resulting in a compact flame. More importantly, evidence of ARS changing the shear layer dynamics by disturbing the flow field upstream to the step is presented.

Numerical Formulation

The schematic of the problem pertaining to a dump combustor is shown in Fig. 1. The flow/combustion field is modelled in a shorter length scale h and longer (convective) time scale $t = h/u$, whereas the acoustics is modelled in a longer length scale L (for longitudinal acoustic modes) and shorter time scale $\tau = L/c$. h is characteristic of the lateral dimensions of the combustor, such as the step height, and L is the length of the combustor. u and c are reference flow and sound speeds. The fluid is considered to be a calorically perfect gas and all the diffusion coefficients are assumed to be equal and constant. The conservation equations are non-dimensionalised with shorter length and time scales, h and τ respectively [21]. Apart from other non-dimensional quantities, the resulting set of equations have $M = u/c$ and h/L, the Mach number and the ratio of length scales respectively. Taken together, these constitute the simultaneous multiple length and time scales. Both of these quantities are taken to be unequally small in general, here. To handle two small parameters simultaneously, each of them is, in turn, represented as a function of a single small number ε through the relations $M = \varepsilon^m$ and $h/L = \varepsilon^n$. Here, we choose $m = 1$ and let n evolve in the solution as an indicator of the compactness of the flame due to acoustic coupling.

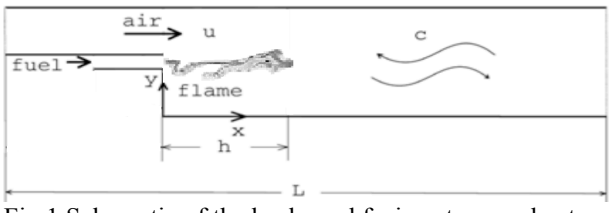

Fig.1 Schematic of the backward facing step combustor.

Any dependent variable φ is expanded according to the ansatz $\varphi = \sum_i \varepsilon^i \varphi_i$. For $m = 1$, this is the conventional Mach number expansion, with M as the small parameter. Splitting the spatial and temporal derivatives for the two scales considered, expanding the variables as powers of ε and comparing equi-order terms in ε, we decompose the conservation equations for the flow and acoustics in their respective length and time scales. In the resulting set of equations, it is observed that both the flow and acoustics affect the fluid velocity to leading order. Temporally averaging the base-flow equations and spatially averaging the acoustic equations results in the definition of new velocity variables that can be identified distinctly with the base flow and the acoustics. The averaging also results in the appearance of explicit interaction terms between the base-flow and acoustics. The final sets of conservation equations for the flow and acoustics are given below [21]:

Flow:

$$\frac{\partial \rho_0}{\partial t} + \frac{\partial}{\partial x_i}\left(\rho_0 \overline{u_{0j}}^{\tau}\right) = 0 \tag{1}$$

$$\frac{\partial}{\partial t}\left(\rho_0 \overline{u_{0i}}^{\tau}\right) + \frac{\partial}{\partial x_j}\left(\rho_0 \overline{u_{0i}}^{\tau}\overline{u_{0j}}^{\tau}\right) + \frac{1}{\gamma}\frac{\partial \overline{p_2}^{\tau}}{\partial x_i} - \frac{1}{Re}\left(\frac{\partial^2 \overline{u_{0i}}^{\tau}}{\partial x_j^2} + \frac{1}{3}\frac{\partial}{\partial x_i}\left(\frac{\partial \overline{u_{0k}}^{\tau}}{\partial x_k}\right)\right) = -\frac{\partial}{\partial x_j}\left(\rho_0 \overline{u_{0i}'^{\tau} u_{0j}'^{\tau}}\right) \tag{2}$$

$$\frac{dp_0}{dt} + \gamma p_0 \frac{\partial \overline{u_{0j}}^{\tau}}{\partial x_j} = (\gamma - 1) Da Q_{R0} + \frac{\gamma}{Pe}\frac{\partial^2 T_0}{\partial x_j^2} \tag{3}$$

$$\frac{\partial \rho_{K0}}{\partial t} + \frac{\partial}{\partial x_j}\left(\rho_{K0}\overline{u_{0j}}^{\tau}\right) - \frac{1}{ReSc}\frac{\partial^2 \rho_{K0}}{\partial x_j^2} - Da_K \omega_K = 0 \tag{4}$$

$$p_0 = \rho_0 T_0 \tag{5}$$

Acoustics:

$$\frac{\partial \rho_1}{\partial \tau} + \frac{\partial}{\partial \xi_j}\left(\overline{\rho_0}^{x} u_{0j}'^{\tau}\right) = -\frac{\partial}{\partial \xi_j}\left(\overline{\rho_0}^{x}\overline{\overline{u_{0j}}^{\tau}}^{x} + \overline{\rho_0'^{x}\overline{u_{0j}}^{\tau\prime x}}^{x}\right) \tag{6}$$

$$\overline{\rho_0}^{x}\frac{\partial u_{0i}'^{\tau}}{\partial \tau} + \frac{1}{\gamma}\frac{\partial p_1}{\partial \xi_i} = 0 \tag{7}$$

$$\frac{\partial p_1}{\partial \tau} + \gamma p_0 \frac{\partial u_{0j}'^{\tau}}{\partial \xi_j} = -\gamma p_0 \frac{\partial \overline{\overline{u_{0j}}^{\tau}}^{x}}{\partial \xi_j} \tag{8}$$

$$\frac{\partial \overline{\rho_{K1}}^{x}}{\partial \tau} + \frac{\partial}{\partial \xi_j}\left(\overline{\rho_{K0}}^{x} u_{0j}'^{\tau}\right) = -\frac{\partial}{\partial \xi_j}\left(\overline{\rho_{K0}}^{x}\overline{\overline{u_{0j}}^{\tau}}^{x} + \overline{\rho_{K0}'^{x}\overline{u_{0j}}^{\tau\prime x}}^{x}\right) \tag{9}$$

$$p_1 = \rho_1 \overline{T_0}^{x} + \overline{\rho_0}^{x} T_1 \tag{10}$$

In these equations, ρ_0, $\overline{u_{0j}}^{\tau}$, $\overline{p_2}^{\tau}$, ρ_{K0} and T_0 are the mixture density of the base flow, velocity, pressure (hydrodynamic), partial density of species K and temperature respectively and ρ_1, $u_{0j}'^{\tau}$, p_1, ρ_{K1} and T_1 are the corresponding acoustic quantities. *Re, Pe, Sc,* Da and Da_K, are the Reynolds, Peclet, Schmidt, Damköhler and Damköhler for species K respectively. With these variables and non-dimensional quantities, Eqns.(1)–(5) can be identified as the Navier-Stokes equations for the incompressible flow with the temperature-dependentdensity governing the combustion zone, and Eqns. (6)–(10) as the linearized Euler equations governing the acoustic zone. Explicit coupling terms, viz., the flow divergence over acoustic length scale (RHS of Eqn.(8))and the acoustic Reynolds stress (ARS, RHS of Eqn. (2)) are brought out naturally without any ad hoc treatment.

In this formulation, the acoustic damping does not show up. This is because, the length scale associated with the acoustic boundary layer where most of the damping occurs is not considered. Besides, bulk of the acoustic losses could occur at the boundaries, which are not governed by the above equations. Accounting for acoustic damping is important to predict the long-time behaviour of the system and eventually predict the limit

cycle amplitude of the system. The above formulation is extended to include acoustic damping by considering a visco-thermal friction term [21] in the acoustic momentum balance equation Eqn. (7).

Solution Methodology

Simulations reported in this work are performed using modified versions of open source codes FASTEST [22] and CLAWPACK [23,24], which are employed to solve the base flow (Eqns. (1)-(5)) and acoustic sets of equations (Eq. 7 including the acoustic damping term and Eq. 8).

In FASTEST, the spatial discretization is second order accurate and deferred correction procedure [25] is followed to discretize the convective terms. Flux limiters that blend the first order upwind and second order central differencing schemes depending upon the local distribution of a scalar are also employed. Temporal discretization is performed with second order accurate Crank-Nicolson method. The matrix inversions are performed by the strongly implicit procedure (SIP) [25].In all the acoustic computations reported in the present work, the first order Gudunov-split method is employed [26].

Turbulence in the flow is handled by means of LES, and the sub-grid scale (SGS) terms (including the TAI terms) are simulated by adopting the monotonically implicit LES (MILES) approach [21]. A single step global chemical reaction is adopted with laminar finite-rate Arrhenius kinetics to compute the production rate of species.

In-house benchmarks are performed using FASTEST to compute flow through backward facing step [27, 28] and channel flows [29]. Its capability to compute incompressible variable density flow is validated following [30]. CLAWPACK is tested to reproduce the duct natural frequencies in the presence of mean temperature gradient [31].

The acoustic damping is the only aspect that is modelled in an *ad hoc* fashion and together with this the strength of the dilatation, driving the acoustics is artificially tuned to calibrate for acoustic amplitudes against the experimental data.

Both the flow and acoustic computations are performed in MPI-based parallel environment. MPI-based specialized modules are added that can perform spatial/temporal averaging and interpolation of flow quantities from the flow grid to the acoustic grid and vice-versa. Quadratic Shepard scheme is used to perform data interpolation in 3D [32]. A total of 34 processors spread across two nodesare used to perform a coupled simulation.

Results and Discussion

The length of the combustor is 1.4 m and the step plane is located 0.4 m from the inlet. The step height h = 0.03 m and the expansion ratio across the step plane is 2. The span-wise extent of the duct is 0.06 m. Coupled 3D simulations are performed for *Re*in the range of 18000-50000, at a fixed fuel flow rate of 142 mg/s, for which experimental data on acoustic pressure measurements are available for direct comparison [15].

A reduced domain of 0.15 m and 0.4 m (5h and 13h) upstream and downstream of the step plane respectively is considered for turbulent combustion computations. The range of scales expected in terms of non-dimensional wave number k for Re = 18000 and 33000 are $1.0\text{-}1.5\times10^3$ and $1.0\text{-}2.5\times10^3$ respectively. Multi-block structured mesh with a total size of 1.04 million nodes is used.

Random inlet velocity perturbations with amplitude of 20% of the mean inlet velocity are superposed on the mean velocity and are prescribed at the inlet plane. No-slip boundary condition is used at the walls. Outflow boundary condition is used at the exit plane of the computational domain. At the exit plane, the velocity is corrected such that instantaneous balance in volume flow rate is satisfied taking into account the dilatation that occurs in the computational domain, to improve global convergence. The walls of the combustor are maintained at 700 K as an approximation of hot walls witnessed in the experiments. Properties for all the species are kept constant with reference to atmospheric conditions. The inlet temperature at both the ducts is specified as 298 K corresponding to experiments. The thermodynamic pressure is taken as 101325 Pa. A simplified reaction of the form F + 3O + 12N → 4P + 12N is considered. The molecular weight of all the species is taken equal as 28 kg/kmol. The reaction rate is taken to be of Arrhenius type and the pre-exponential factor and activation temperature are taken as 3.3×10^{12} $(\text{gmol/cm})^{(1-\upsilon_1-\upsilon_2)}/\text{s}$ and 2300 K; υ_1 and υ_2 are the exponents in the rate equation for the fuel and oxidiser (air) species respectively and are taken as 0.15 and 1.15 respectively. The calorific value of the fuel is taken as 50 MJ/kg. Most of the parameters are chosen such that the process closely resembles methane-air combustion overall.

For the acoustic computations, the entire length of the duct as in the experiment is considered as the domain, and an uniform grid with a spatial resolution of ~8 mm is employed. An open-open boundary condition is prescribed at the inlet and exit planes of the duct; other surfaces are treated as walls. The flow properties and the acoustic source are spatially averaged in 3D over half the step height as the reference flow length scale and communicated to the acoustic solver. Upstream of the embedded domain, they are taken as constant corresponding to the experimental conditions at 298 K. In the embedded region, they are communicated at the start of every flow time step. For the downstream part, the flow domain's exit plane average properties are computed and communicated to the acoustic solver at the start of every flow time step.

All the computations reported in this work are calibrated against experimental data [15] by introducing factors that modify the acoustic source and damping (rhs of Eq. (8) and Eq. (11) respectively). These are kept as 0.4 and 40 respectively.

From Fig. 2(a), it is seen that the shift from constant He to a linearly increasing trend corresponding to the lock on of the duct acoustic mode to the vortex shedding mode (St=0.2 [15]) is captured by the coupled simulations at a relatively lower Reynolds number (Re=26000) to that in the experiments [15] (Re=31000). There is a good match in the computed St with that of the experiments [15]. The combustion-acoustic lock-on is characterized by nonlinear variation in the pressure amplitude, a trend that the coupled computations are able to predict quite well (Fig. 2(c)). Exact match in the amplitudes is a matter of fine-tuning the calibration on damping, but the key features are the frequency shift accompanied by a non-linear amplitude variation with Reynolds number corresponding to lock-on.

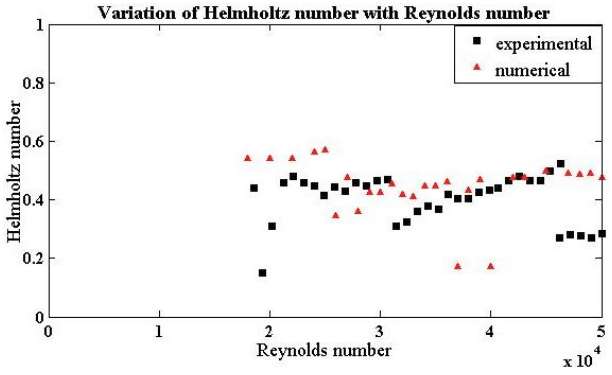

(a)

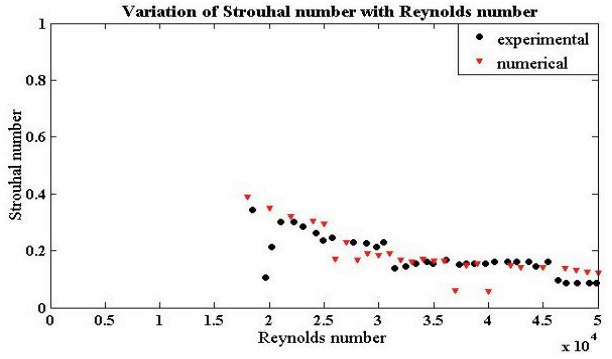

(b)

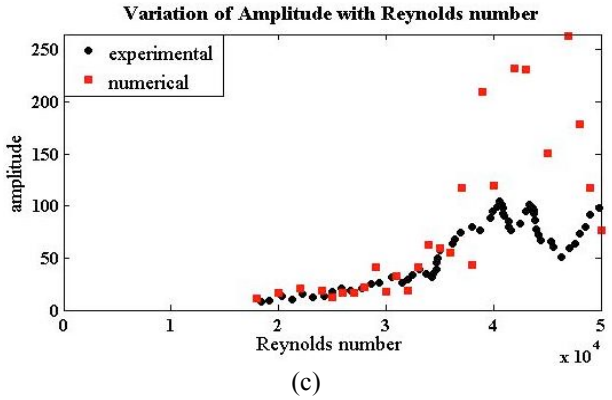

(c)

Fig.2(a) Variation of Helmholtz number with Re, showing lock-on and the corresponding (b) variation in Strouhal number and (c) the non-linear variation in pressure amplitude with Re along the top wall downstream of the step.

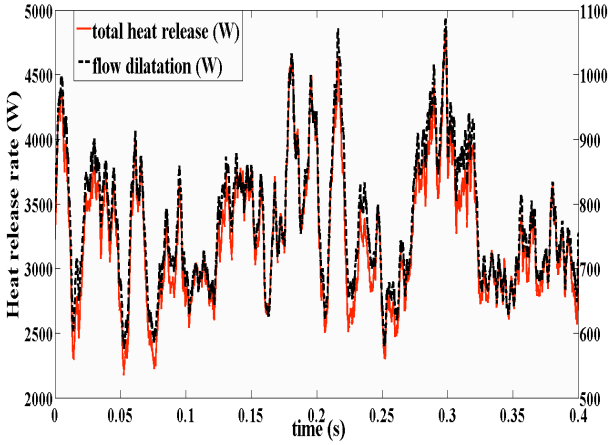

(a)

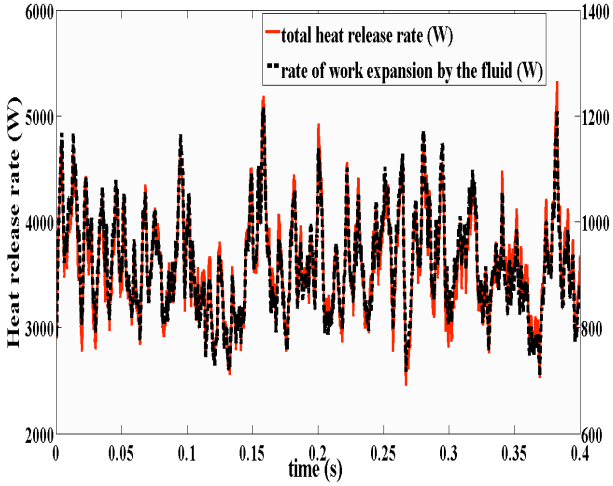

(b)

Fig.3 Time evolution of total heat release rate and rate of work expansion by the fluid (flow dilatation) of Re=18000 (before lock-on) and Re=33000 (after lock-on) coupled combustion.

Fig.3 explains the time evolution of total heat release rate and flow dilatation of Re=18000 and Re=33000 coupled combustion. Before lock-on (Fig. 4(a)), there is no significant role played by ARS in the combustion zone as the total heat release rate and flow dilatation are very low and moreover, there is a noticeable disparity between the total heat release rate and flow dilatation but after lock-on, there is not only a strong match between them indicating a strong acoustic source, but also high heat release rate fluctuations, which indicate the intense mixing caused by ARS (further discussed next) as the time scales approach each other.

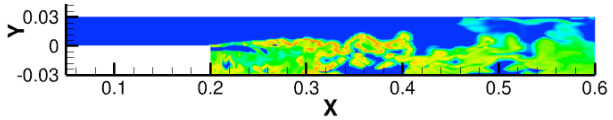

(a)

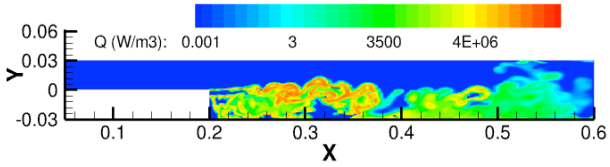

(b)

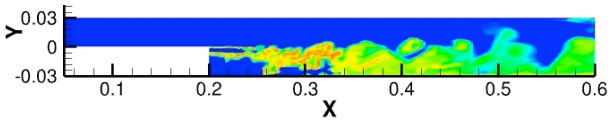

(c)

Fig. 4 Heat release rate contours of (a) Re=18000, (b) Re = 33000 coupled and (c) Re=33000 uncoupled combustion – mid-span of the combustor.

In the coupled simulations, Re=18000 and Re=33000 are compared to explain the significance of ARS action with increase in Re and as a consequence of lock-on. Large-scale roll up is eminent in Fig. 4(b) as expected and combustion occurs predominantly in the vortical structures unlike in Re=18000 (Fig. 4(a)) where there is a relatively lengthy flame with the absence of large-scale vortical structures.

In order to comprehend the effect of acoustics on the flow field, the coupled case should be compared with that of an acoustically decoupled flow. Fig.4(c) explains such a situation for Re=33000, wherein the flame is farther from the step with absence of any large-scale roll up. Interestingly, the coupled simulations show a shear-layer roll up towards the top which is absent in the uncoupled combustion of Re=33000. To further illustrate the disturbance of the shear layer in the coupled case, Z-component of vorticity contours (owing to XY plane symmetry) are considered as shown in Fig. 5.It is evident from Fig. 5(b) that the flow field upstream to the step has a dominant anti-clockwise vorticity while the uncoupled case has opposing vorticity that continue till the step location. The vorticity behavior in the coupled case is further bolstered by the contour of Z component of torque exerted by ARS as shown in Fig.6. As can be seen, ARS torque disturbs the upstream flow field by inducing an anti-clockwise rotation. The flow continues to driftfurther away from the step, but the torque exerted by ARS causes intense mixing between reactants by inducing appropriate rotation such that the fuel is mixed with air and vice-versa resulting in the shear layer rolling upwards.

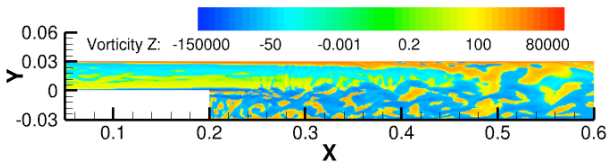

(a)

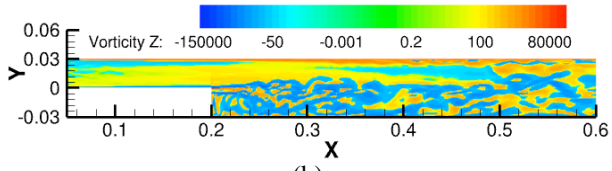

(b)

Fig.5 Contour of Z component of Vorticity field of Re=33000 (a) uncoupled and (b) coupled combustion.

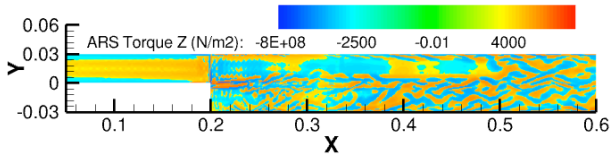

Fig.6 Contour of Z component of Torque exerted by ARS of Re=33000.

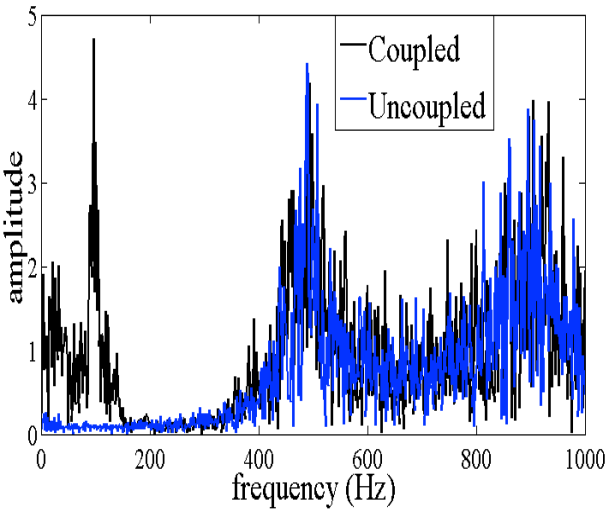

Fig.7FFT spectra of hydrodynamic pressure of Re=33000 coupled and uncoupled combustion at x/h=−2.

Fig. 7 shows the FFT spectra of hydrodynamic pressure monitored at the upstream location of x/h=−2 for Re=33000 coupled and uncoupled combustion. Evidently, the dominant vorticity in the upstream flow field of the coupled case correspond to the vortex shedding frequency (St ~ 0.2) observed near the top wall, downstream, indicating that it is prevalent in the combustor as the time scales approach each other, hence causing the lock-on.

Conclusion

The present work adopts an approach of simultaneous multiple time and length scales of flow and acoustics to demonstrate that the time scales actually hasten to approach each other in a lock-on, leading to combustion instability, rather than presume equal time scales of the two processes à priori in an ad hoc manner. The Flow-acoustic lock on happens at a relatively lower Reynolds number to that of the experiments. However, there is a very good match in St with Re and the non-linear variation of amplitude with Re after lock on is also captured.

As the time scales approach each other, there is high amplitude heat release rate fluctuations followed by a strong match between the heat release rate and flow dilatation which happens due to ARS causing intense mixing by churning large-scale vortical structures, hence engendering a compact flame.

ARS changes the shear layer dynamics by inducing significant vorticity upstream of the step, a phenomenon that is absent in an acoustically decoupled flow. The upstream vorticity frequency corresponds to that of thedominant vortex shedding frequency that is observed near the top wall downstream indicating their prevalence in the combustor during instability mode.

Hence, the present approach brings out rich physics of the problem, and is a computationally affordable alternative to predict combustion instability in turbulent reacting flows in ducted geometries.

Acknowledgements

This work was partly supported by the Deutsche Forschungsgameinschaft. The Department of Science and Technology, Government of India supports the National Centre for Combustion Research and Development (NCCRD). Thanks are also due to the High Performance Computing Environment (HPCE) of Indian Institute of Technology Madras for providing the resources for computations.

References

[1] S. C. Schadow and E. J. Gutmark, Prog. Energy Combust. Sci. 18 (1992) 117-132.

[2] T. C. Lieuwen and B. T. Zinn, Proc. Combust. Inst. 27 (2) (1998) 1809-1816.

[3] T. J. Poinsot and S. M. Candel, Combust. Sci. Technol. 61 (1988) 121-153.

[4] S. Menon and W. H. Jou, Combustion Sci. and Tech. 75 (1991) 53-72.

[5] S. J. Brookes and R. S. Cant and I. D. J. Dupere and A. P. Dowling, J. Eng. Gas Turbines Power 123 (2) (2001) 322-326.

[6] Y. Huang and V. Yang, Combust. Flame 136 (3) (2004) 383-389.

[7] S. Roux and G. Lartigue and T. J. Poinsot and U. Meier and C. Bérat, Combust. Flame 141 (2005) 40-54.

[8] L. Selle and L. Benoit and T. Poinsot and F. Nicoud and W. Krebs, Combust. Flame 145 (2006) 194-205.

[9] F. Boudy and D. Durox and T. Schuller and S. M. Candel, Proc. Combust. Inst. 33 (1) (2011) 1121-1128.

[10] F. E. C. Culick, Combustion instabilities in liquid-fuelled propulsion system--An Overview, AGARD-CP-450, 1988.

[11] J. D. Sterling, Nonlinear analysis and modelling of combustion instabilities in a laboratory combustor, Combust. Sci. Technol. 89 (1993) 167-179.

[12] K. I. Matveev and F. E. C. Culick, A model for combustion instability involving vortex shedding, Combust. Sci. Technol. 175 (6) (2003) 1059-1083.

[13] G. Searby, Acoustic instability in premixed flames, Combust. Sci. Technol. (81) (1992) 221-231.

[14] R. Balachandran and S. R. Chakravarthy and R. I. Sujith, J. Propul. Power 24 (6) (2008) 1382-1389.

[15] S. R. Chakravarthy and O. J. Shreenivasan and B. Böhm and A. Dreizler and J. Janicka, J. Acou. Soc. Am. 122 (1) 120-127.

[16] X. Wu and M. Wang and P. Moin and N. Peters, J. Fluid Mech. 497 (2003) 22-53.

[17] M. Tyagi and S. R. Chakravarthy and R. I. Sujith, Combust. Theo. Modelling 11(2) (2007) 205-226.

[18] W. L. Nyborg, Acoustic Streaming. In Physical Acoustics Part B (ed. W. P. Mason, II), Academic Press, 1965.

[19] J. Lighthill, J. Sound Vib., 61 (3) (1978) 391-418

[20] M. Tanabe and T. Morita and K. Aoki and K. Satoh and T. Fujimori and J. Sato, Proc. Combust. Inst., 28 (2000) 1007-1013.

[21] S. R. Chakravarthy and C. Balaji and R. K. R. Katreddy and A. Nath, n3l - Int'l Summer School and Workshop on Non-Normal and Nonlinear Effects in Aero- and Thermoacoustics, 2013.

[22] FASTEST, available at http://www.fnb.tu.darmstadt.de/forschung_fnb/software_fnb/software_fnb.en.jsp .

[23] CLAWPACK, available at http://www.amath.washington.edu/~claw/ .

[24] R. J. Leveque, J. Comput. Phys., 131 (1997) 327-353.

[25] J. H. Ferziger and M. Peric, Computational methods for fluid dynamics, Springer, 2002.

[26] R. J. Leveque, Finite volume methods for hyperbolic problems, Cambridge, 2002.

[27] B. F. Armaly and F. Durst and J. C. F. Pereira and Schonung, J. Fluid Mech., 123 (1983) 473-496.

[28] R. Friedrich and M. Arnal, J. Wind Eng. Ind. Aerodyn., 35 (1990) 101-128.

[29] A. K. M. F. Hussain and W. C. Reynolds, J. Fluid Engg., (1975) 568-580

[30] F. Nicoud, J. Comput. Phys., 159 (2000) 71-97

[31] R. I. Sujith and G. A. Waldherr and B. T. Zinn, J. Sound Vib., (1995) 389-402

[32] R. J. Renka, ACM Trans. Math. Softw., 1988, 151-152.